Journal of the Brazilian Society of Mechanical Sciences and Engineering (2018) 40:422
https://doi.org/10.1007/s40430-018-1353-8

TECHNICAL PAPER

Activation energy and chemical reaction in Maxwell magneto-nanoliquid with passive control of nanoparticle volume fraction

G. K. Ramesh[1] · S. A. Shehzad[2] · T. Hayat[3,4] · A. Alsaedi[4]

Received: 28 March 2018 / Accepted: 10 August 2018 / Published online: 16 August 2018
© The Brazilian Society of Mechanical Sciences and Engineering 2018

Abstract
Two-dimensional flow of Maxwell magneto-nanoliquid by stretching surface is investigated. Convective boundary conditions and passive control of nanoparticles volume fraction are used for the analysis of thermal and concentration boundary layers. Flow analysis is created by considering Buongiorno model. Influences of activation energy and chemical reaction are useful application in lubrication practice, oil and water emulsions; therefore, we retained these effects. The differential framework is illustrated numerically via spectral relaxation method. Part of critical parameters on flow fields and additionally on the skin fiction factor and energy and mass transportation rates are resolved and discussed.

Keywords Activation energy · Chemical reaction · Maxwell nanoliquid · Convective condition · Spectral relaxation method

1 Introduction

Analysis of non-Newtonian liquids is important due to its involvement in current applications. Such examples include blood at low sheer rate, emulsion, mud, chyme, organic product purée, chemicals, sugar game plan and shampoos. No single equation can predict the diverse characteristics of non-Newtonian materials. Thus, different logical models have been proposed by the researchers. Maxwell is one subclass of rate-type fluids. This fluid model predicts time relaxation impacts. Such effects cannot be expected by differential fluids. Maxwell liquid model is particularly helpful for polymers of low molecular weight. Fetecau and Fetecau [1] obtained analytical solution of flow of Maxwell liquid bounded by an infinite plate. Some current investigations predicting flow of Maxwell liquid have been elucidated in Refs. [2–9].

Nanoliquids can massively help the heat exchange qualities of working liquids. The heat transport wonder is a crucial procedure in designing and in this manner improvement in heat exchange angles prompts to propel the productivity of bunches of procedures. In like manner, the nanoliquids have a few applications for example as coolants, heat exchangers, sun-based water warming, cooling of electronic types of gear, chillers, icebox coolers, space vehicles, atomic reactors, smaller scale channel heat sinks and ointments. Nanofluid term was right off the bat presented by Choi [10]. From there on, test and hypothetical examinations on nanofluid's heat exchange perspectives are finished by Buongiorno [11]. Afterward, much information has been presented on this topic can be found in Refs. [12–25]. The magneto-nanoliquids are the liquids that have both magnetic and fluid qualities. These materials have pivotal part in optical switches, modulators, optical gratings and especially in optical fiber channels. The attractive nanoparticles are very noticeable in pharmaceutical, disease treatment, tumor investigation, sink drift partition and many more. The current takes a shot at magneto-nanofluids are exhibited in Refs. [26–30].

Activation energy can be portrayed as the tiniest required imperativeness that reactants must get before a substance reaction can happen. Mass transport process by

Technical Editor: Cezar Negrao.

✉ S. A. Shehzad
ali_qau70@yahoo.com

[1] Department of Mathematics, K.L.E'S J.T. College, Gadag 582101, Karnataka, India

[2] Department of Mathematics, COMSATS University Islamabad, Sahiwal 57000, Pakistan

[3] Department of Mathematics, Quaid-I-Azam University, Islamabad 44000, Pakistan

[4] NAAM Research Group, Department of Mathematics, Faculty of Science, King Abdulaziz University, Jeddah 21589, Saudi Arabia

substance reaction with approving essentialness routinely met in applications including mechanics of water and oil emulsions, geothermal supplies, compound portraying and sustenance getting ready. Makinde et al. [31] addressed the heat transport behavior in porous flat plate by considering the effect of radiation and activation energy. Maleque [32] examined the exothermic and endothermic chemical reactions in MHD viscous liquid by considering Arrhenius activation energy. Awad et al. [33] elaborated binary chemical reaction and activation energy in an unsteady rotating fluid. Casson liquid flow past a stretching and shrinking surface with binary chemical reaction was numerically analyzed by Abbas et al. [34]. Shafique et al. [35] studied the flow of Maxwell liquid in rotating frame with activation energy and chemical reaction. Mustafa et al. [36] present the magneto-nanoliquid over a vertical sheet by accounting the activation energy and chemical reaction.

Convective point of confinement condition is mostly used to describe a direct convective heat exchange condition for no less than one scientific component in heat. Heat transport examination with convective point of confinement conditions is evoked in methodology, for instance, heat essentialness storing, gas turbines and nuclear plants. In context of the above examination, Aziz [37] studied the heat transport phenomenon in boundary layer flow by taking convective-type boundary condition. His study reveals that similarity solutions are possible only when convective heat transport associated with the hot liquid on the lower sheet surface is proportional to $x^{-1/2}$. Numerous scientists [38–42] have examined the flow and heat transfer of viscous/non-Newtonian fluids via convective-type boundary condition.

In the above literatures and applications, we noted that activation energy can be realized as energy barrier that separates two minima of potential energy which has to be overcome by reactants to initiate a chemical reaction. So that we are going to analyze the chemical reaction and activation energy effects in Maxwell nanoliquid flow. The aspects of Brownian movement and thermophoretic are retained due to consideration of nanofluid model. The problem is dealt with convective boundary condition and passively controlled mass flux. The transformed non-dimensional equations are solved numerically using spectral relaxation scheme because it gives a better accuracy on coarser grids which significantly improves the speed of the convergence. Validation of computations has been visualized through comparative benchmark.

2 Statement of problem

Model of the problem is presented in Fig. 1. Here steady two-dimensional Maxwell liquid flow by stretching surface is considered. Here the flow occupies to $y > 0$, sheet velocity $U_w(x) = bx$, $b > 0$ and x-axis taken along the sheet. Uniform magnetic field B_0 is applied normal to the sheet. Influences of activation energy and chemical reaction are accounted in mass transfer. Convective surface temperature is denoted by T_f, and heat transport coefficient is h_f. Nanoparticles normal flux at the surface is passively controlled. Under the above assumptions, the rheological model of continuity, momentum, energy and mass equations are

$$\nabla \cdot V = 0, \tag{1}$$

$$\rho_f (V \cdot \nabla) V = -\nabla p + \nabla \cdot S, \tag{2}$$

$$\rho_p c_p (V \cdot \nabla T) = k \nabla^2 T + \rho_f c_f \left[D_B \nabla C \cdot \nabla T + \frac{D_T}{T_\infty} (\nabla T)^2 \right], \tag{3}$$

$$(V \cdot \nabla C) = D_B \nabla^2 C + \frac{D_T}{T_\infty} \nabla^2 T - k_r^2 (C - C_\infty) \left(\frac{T}{T_\infty} \right)^n \exp\left(\frac{-Ea}{\kappa T} \right). \tag{4}$$

From Eq. (2), last term S represents the extra stress tensor and for Maxwell fluid, it satisfies $S + \lambda_1 \frac{DS}{Dt} = \mu A^*$. Here $A^* = \nabla V + (\nabla V)^t$ for first Rivlin–Ericksen tensor, λ_1 for time relaxation of liquid. Also third term on RHS of Eq. (4) represents modified Arrhenius formula in which k_r^2 for rate of reaction [35], Ea for activation energy, κ for Boltzmann constant and n dimensionless fitted rate constant which lies in the range $-1 < n < 1$.

After the boundary layer approximations, one has [26, 29]:

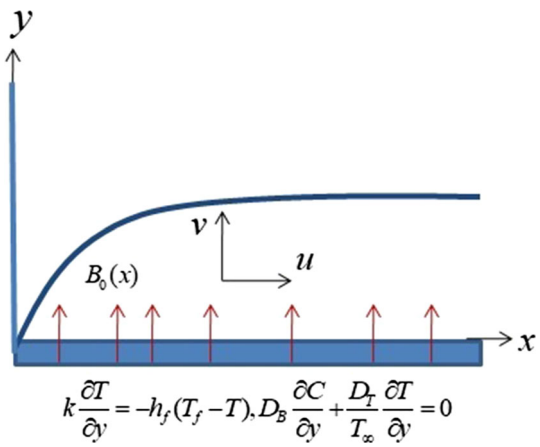

Fig. 1 Flow model and coordinate system

$$\frac{\partial u}{\partial x}+\frac{\partial v}{\partial y}=0, \tag{5}$$

$$u\frac{\partial u}{\partial x}+v\frac{\partial u}{\partial y}=v\frac{\partial^2 u}{\partial y^2}+k_0\left(u^2\frac{\partial^2 u}{\partial x^2}+v^2\frac{\partial^2 u}{\partial y^2}+2uv\frac{\partial^2 u}{\partial x\partial y}\right)-\frac{\sigma B_0^2}{\rho}\left(u+k_0 v\frac{\partial u}{\partial y}\right) \tag{6}$$

$$u\frac{\partial T}{\partial x}+v\frac{\partial T}{\partial y}=\alpha\left(\frac{\partial^2 T}{\partial y^2}\right)+\tau\left\{D_{\mathrm{B}}\left(\frac{\partial C}{\partial y}\frac{\partial T}{\partial y}\right)+\left(\frac{D_T}{T_\infty}\right)\left[\left(\frac{\partial T}{\partial y}\right)^2\right]\right\}, \tag{7}$$

$$u\frac{\partial C}{\partial x}+v\frac{\partial C}{\partial y}=D_{\mathrm{B}}\frac{\partial^2 C}{\partial y^2}+\left(\frac{D_T}{T_\infty}\right)\left(\frac{\partial^2 T}{\partial y^2}\right)-k_{\mathrm{r}}^2(C-C_\infty)\left(\frac{T}{T_\infty}\right)^n\exp\left(\frac{-Ea}{\kappa T}\right), \tag{8}$$

Imposed boundary conditions are [40]:

$$\begin{aligned}&u=U_{\mathrm{w}}(x),\quad v=0,\quad -k\frac{\partial T}{\partial y}=h_{\mathrm{f}}(T_{\mathrm{f}}-T),\\&D_B\frac{\partial C}{\partial y}+\frac{D_T}{T_\infty}\frac{\partial T}{\partial y}=0\ (\text{passive control of }\phi)\ \text{at } y=0\\&u\to 0,\quad T\to T_\infty,\quad C\to C_\infty \text{ as } y\to\infty\end{aligned} \tag{9}$$

Defined variables [15, 17]:

$$\varsigma=\left(\frac{U_{\mathrm{w}}}{vx}\right)^{1/2}y,\quad f(\varsigma)=\frac{\psi}{(xvU_{\mathrm{w}})^{1/2}},\quad \theta(\varsigma)=\frac{T-T_\infty}{T_{\mathrm{f}}-T_\infty},\quad \phi(\varsigma)=\frac{C-C_\infty}{C_\infty}(\text{passive control of }\phi) \tag{10}$$

and making use of (10), Eqs. (5–8) are reduced to following non-dimensional equations

$$\frac{\mathrm{d}^3 f}{\mathrm{d}\varsigma^3}+f\frac{\mathrm{d}^2 f}{\mathrm{d}\varsigma^2}-\left(\frac{\mathrm{d}f}{\mathrm{d}\varsigma}\right)^2-M^2\frac{\mathrm{d}f}{\mathrm{d}\varsigma}+MKf\frac{\mathrm{d}^2 f}{\mathrm{d}\varsigma^2}+K\left(f^2\frac{\mathrm{d}^3 f}{\mathrm{d}\varsigma^3}-2f\frac{\mathrm{d}f}{\mathrm{d}\varsigma}\frac{\mathrm{d}^2 f}{\mathrm{d}\varsigma^2}\right)=0, \tag{11}$$

$$\frac{1}{\mathrm{Pr}}\frac{\mathrm{d}^2\theta}{\mathrm{d}\varsigma^2}+f\frac{\mathrm{d}\theta}{\mathrm{d}\varsigma}+Nb\frac{\mathrm{d}\theta}{\mathrm{d}\varsigma}\frac{\mathrm{d}\phi}{\mathrm{d}\varsigma}+Nt\left(\frac{\mathrm{d}\theta}{\mathrm{d}\varsigma}\right)^2=0, \tag{12}$$

$$\frac{\mathrm{d}^2\phi}{\mathrm{d}\varsigma^2}+Scf\frac{\mathrm{d}\phi}{\mathrm{d}\varsigma}+\frac{Nt}{Nb}\frac{\mathrm{d}^2\theta}{\mathrm{d}\varsigma^2}-Sc\sigma(1+\delta\theta)^n\phi\exp\left(\frac{-E}{1+\delta\theta}\right)=0. \tag{13}$$

Corresponding boundary conditions become

$$\begin{aligned}&f(\varsigma)=0,\quad \frac{\mathrm{d}f}{\mathrm{d}\varsigma}=1,\quad \frac{\mathrm{d}\theta}{d\varsigma}=-Bi(1-\theta(\varsigma)),\\&Nb\frac{\mathrm{d}\phi}{\mathrm{d}\varsigma}+Nt\frac{\mathrm{d}\theta}{\mathrm{d}\varsigma}=0\ \text{at}\ \varsigma=0\\&\frac{\mathrm{d}f}{\mathrm{d}\varsigma}\to 0,\quad \theta(\varsigma)\to 0,\quad \phi(\varsigma)\to 0\ \text{as}\ \varsigma\to\infty\end{aligned} \tag{14}$$

Here key parameters of the extended study are M—Hartmann number, K—elastic parameter, Pr—Prandtl number, Nb—Brownian movement, Nt—thermophoretic, Sc—Schmidt number, Bi—Biot number, σ—reaction rate, E—activation energy and δ—temperature difference. These can be expressed as

$$\begin{aligned}&M=\frac{\sigma B_0^2}{\rho b},\quad K=bk_0,\quad \mathrm{Pr}=\frac{v}{\alpha},\quad Nb=\frac{\tau D_{\mathrm{B}}C_\infty}{v},\quad Nt=\frac{\tau D_T(T_{\mathrm{w}}-T_\infty)}{vT_\infty},\\&Sc=\frac{v}{D_{\mathrm{B}}},\quad \sigma=\frac{k_{\mathrm{r}}^2}{b},\quad E=\frac{Ea}{\kappa T_\infty},\quad \delta=\frac{T_{\mathrm{w}}-T_\infty}{T_\infty},\quad Bi=\left(\frac{v}{b}\right)^{1/2}\frac{h_{\mathrm{f}}}{k}.\end{aligned}$$

The skin friction factor and wall temperature and concentration gradients are defined as

$$C_{\mathrm{f}}=\frac{\tau_{\mathrm{w}}}{\rho_{\mathrm{f}}U_{\mathrm{w}}^2(x)},\quad Nu=\frac{xq_{\mathrm{w}}}{\alpha(T_{\mathrm{w}}-T_\infty)},\quad Sh=\frac{xq_{\mathrm{m}}}{D_{\mathrm{B}}(C_{\mathrm{w}}-C_\infty)}, \tag{15}$$

where τ_{w} is wall shear stress, q_{w} the heat flux and q_m the mass flux, i.e.,

$$\tau_{\mathrm{w}}=\mu(1+K)\left(\frac{\partial u}{\partial y}\right)_{y=0},\quad q_{\mathrm{w}}=-k\left(\frac{\partial T}{\partial y}\right)_{y=0},\quad q_{\mathrm{w}}=-D_{\mathrm{B}}\left(\frac{\partial C}{\partial y}\right)_{y=0}. \tag{16}$$

Use of Eq. (10) in (16) yields [45]:

$$\mathrm{Re}_x^{1/2}C_f=(1+K)f''(0),\quad \mathrm{Re}_x^{-1/2}Nu=-\theta'(0),\quad \mathrm{Re}_x^{-1/2}Sh=\frac{Nt}{Nb}\theta'(0). \tag{17}$$

3 Method of solution

The nonlinear Eqs. (11–14) are coupled, and ordinary differential equations and hence numerical solutions via spectral relaxation method are computed. To apply this method, first we set $\frac{\mathrm{d}f}{\mathrm{d}\varsigma}=f'=g$ and the governing Eqs. (11–14) are reduced to

$$f' = g, \tag{18}$$

$$g'' + fg' - g^2 - M^2 g + MKfg' + K(f^2 g'' - 2gg') = 0, \tag{19}$$

$$\frac{\theta''}{\Pr} + f\theta' + Nb\theta'\phi' + Nt\theta'^2 = 0, \tag{20}$$

$$\phi'' + Scf\phi' + \frac{Nb}{Nt}\theta'' - Sc\sigma(1+\delta\theta)^n \exp\left(\frac{-E}{1+\delta\theta}\right)\phi = 0, \tag{21}$$

also the boundary conditions become

$$\begin{aligned} &f(0) = 0,\ g(0) = 1,\ \theta'(0) = -Bi(1-\theta(0)),\\ &\mathrm{Nb}\phi'(0) + Nt\theta'(0) = 0,\\ &g(\infty) \to 0,\ \ \theta(\infty) \to 0,\ \ \phi(\infty) \to 0. \end{aligned} \tag{22}$$

The spectral relaxation iteration procedure for the present problem can be written as

$$f'_{r+1} = g_r, \tag{23}$$

$$(1+Kf_r^2)g''_{r+1} + (1+MK)f_r g'_{r+1} - 2Kg_{r+1}g'_r - M^2 g_{r+1} = g_r^2, \tag{24}$$

$$\frac{\theta''_{r+1}}{\Pr} + f_{r+1}\theta'_{r+1} = -Nt\theta'^2_r, \tag{25}$$

$$\phi''_{r+1} + Scf_{r+1}\phi'_{r+1} - Sc\sigma(1+\delta\theta_{r+1})\exp\left(\frac{-E}{1+\delta\theta_{r+1}}\right)\phi_{r+1} = -\frac{Nb}{Nt}\theta''_{r+1}, \tag{26}$$

$$\begin{aligned} &f_{r+1}(0) = 0,\ g_{r+1}(0) = 1,\ \theta'_{r+1}(0)\\ &= -Bi(1-\theta_{r+1}(0)),\ \ \mathrm{Nb}\phi'_{r+1}(0) + N\theta'_{r+1}(0) = 0,\\ &g_{r+1}(\infty) \to 0,\ \ \theta_{r+1}(\infty) \to 0,\ \ \phi_{r+1}(\infty) \to 0. \end{aligned} \tag{27}$$

Since ς varies from ς_0 to ς_∞, let $\xi = \frac{2\varsigma}{\varsigma_\infty} - 1$ be the domain mapped into the interval $[1, -1]$ and grid points are defined as $\xi_i = \cos\left(\frac{\pi j}{N}\right)$, where N represents the number of grid points and $j = 1, 2, 3, \ldots, N$. Now applying the Chebyshev pseudo-spectral method to the above equations, the following iterative equations are obtained.

$$P_1 f_{r+1} = E_1,\ f_{r+1}(\xi_N) = 0, \tag{28}$$

$$P_2 g_{r+1} = E_2, g_{r+1}(\xi_N) = 1 + \delta g'_{r+1}(\xi_N), g_{r+1}(\xi_0) = 0, \tag{29}$$

$$P_3\theta_{r+1} = E_3, \theta'_{r+1}(\xi_N) = -Bi(1-\theta_{r+1}(\xi_N)), \theta_{r+1}(\xi_0) = 0, \tag{30}$$

$$P_4\phi_{r+1} = E_4, Nb\phi'_{r+1}(\xi_N) + N\theta'_{r+1}(\xi_N) = 0, \phi_{r+1}(\xi_0) = 0, \tag{31}$$

where

$$P_1 = D, \quad E_1 = g_r \tag{32}$$

$$\begin{aligned} P_2 &= D^2 + (1+MK)\mathrm{diag}\, f_{r+1}D + K\mathrm{diag}\, f_r^2 D^2 - (2Kg'_r + M^2)I,\\ E_2 &= g_r^2, \end{aligned} \tag{33}$$

$$P_3 = \frac{D^2}{\Pr} + \mathrm{diag}\, f_{r+1}D,\ E_3 = -Nt\theta'^2_r, \tag{34}$$

$$\begin{aligned} P_4 &= D^2 + Sc\,\mathrm{diag}\, f_{r+1}D - Sc\sigma(1+\delta\theta)^n \exp\left(\frac{-E}{1+\delta\theta}\right)I,\\ E_4 &= -\frac{Nb}{Nt}\theta''_{r+1}. \end{aligned} \tag{35}$$

In the above expressions, I and D represent the identity and differentiation matrices. The above matrix system of equations is solved iteratively with a proper initial guesses of $f_0(\varsigma)$, $g_0(\varsigma)$, $\theta_0(\varsigma)$ and $\phi_0(\varsigma)$. To solve these equations, an in-house code has been developed in MATLAB program and it is successfully validated with the standard benchmark solutions before obtaining the simulations.

4 Results and discussion

First we checked the accuracy of numerical computations. For this case, we made a comparative analysis (see Table 1) with the available literature and found that present results coincide with the results of Khan and Pop [12] and Kandasamy et al. [43]. Also we made a graphical comparison with Makinde and Aziz [44] in the absence of $K = M = E = \delta = \sigma = n$. Further, Table 2 presents the values of wall temperature and concentration gradients for E, δ, σ and n. It is noted that temperature gradient and concentration gradient are increased with larger E but the opposite trend is found for δ, σ and n. Important aspect of this study is Biot number. It is clearly observed from Table 3 that increasing values of Bi(0.1–50) enhance both the wall temperature gradient and wall concentration gradient. Additionally increment of Bi from 100 to 100,000 has just minor impact. Thus, as Bi has so large value then there is no significant changes. The much larger Biot number has no significant impact that at high scale, the influence of heat transfer coefficient is very lesser on temperature of liquid.

Essential key parameter of this model is elastic parameter which is displayed in Fig. 2. It is obviously observed

Table 1 Validation results of the present numerical method

Pr	KhanandPop [12]	Kandasamy et al. [38]	Present Study $-\theta'(0)$
0.7	0.4539	0.4542	0.4582
2	0.9113	0.9114	0.9112
7	1.8954	0.8952	1.8953
20	3.3539	3.3538	3.3538
70	6.4621	6.4621	6.4621

Table 2 Computational values of wall temperature gradient and wall concentration gradient when $Nb = Nt = 0.3$, $\Pr = 7$, $K = M = Bi = 0.5$ and $Sc = 10$

E	δ	σ	n	$\mathrm{Re}_x^{-1/2}Nu$	$\mathrm{Re}_x^{-1/2}Sh$
0	1	1	0.5	− 0.387468	0.387468
1				− 0.388968	0.388968
2				− 0.389711	0.389711
1	0	1	0.5	− 0.389247	0.389247
	1			− 0.388968	0.388968
	2			− 0.388720	0.388720
1	1	0	0.5	− 0.390310	0.390310
		1		− 0.388968	0.388968
		2		− 0.387814	0.387814
0	1	1	0	− 0.389073	0.389073
			0.5	− 0.388968	0.388968
			1	− 0.388857	0.388857

Table 3 Computational values of wall temperature gradient and wall concentration gradient when $Nb = Nt = 0.3$, $\Pr = 7$, $K = M = n = 0.5$, $E = \sigma = \delta = 1$ and $Sc = 10$

Bi	$\mathrm{Re}_x^{-1/2}Nu$	$\mathrm{Re}_x^{-1/2}Sh$
0.1	− 0.09489	0.09489
0.5	− 0.38896	0.38896
2	− 0.86677	0.86677
5	− 1.08975	1.08975
10	− 1.17516	1.17516
50	− 1.24418	1.24418
100	− 1.25271	1.25271
500	− 1.25950	1.25950
1000	− 1.26035	1.26035
5000	− 1.26103	1.26103
10,000	− 1.26111	1.26111
100,000	− 1.26119	1.26119
1,000,000	− 1.26120	1.26120
5,000,000	− 1.26120	1.26120

that expansion of K is to increase the velocity field. Additionally this figure reveals that $K = 0$ gives an outcome for consistent liquid. This increase is due to an enhancement in relaxation time factor which is directly related to K. Figure 3 is plotted to exhibit the impact of Hartmann number on liquid velocity. It demonstrates that expansion of M diminishes the velocity of liquid. This happens due to magnetic force normal to electrically directing liquid which can create drag-like force named as Lorentz force. This force is demonstration in course inverse to that of flow which has tendency to block its movement. Figure 4 demonstrates the impacts of M and K on skin friction coefficient. It is noticed that for higher estimations of K, the skin friction coefficient displays the amplifying conduct relating to the increasing estimations of M.

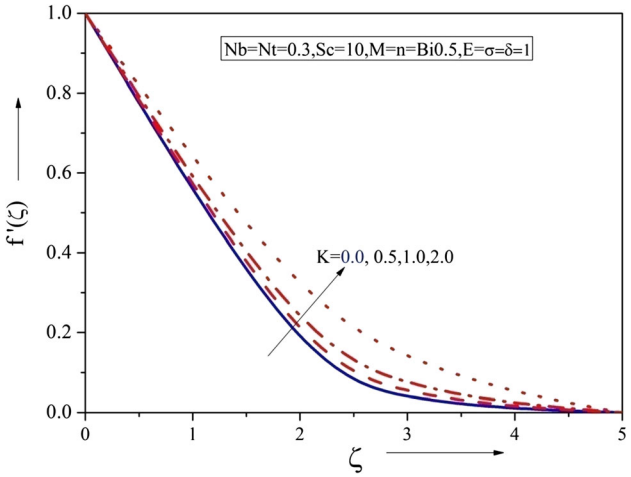

Fig. 2 Effect of K on velocity field

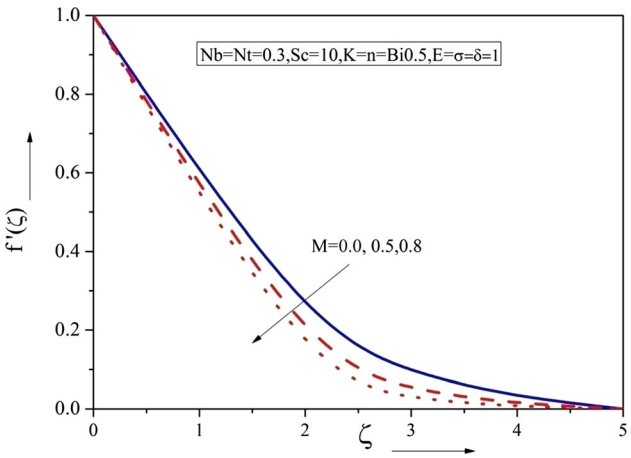

Fig. 3 Effect of M on velocity field

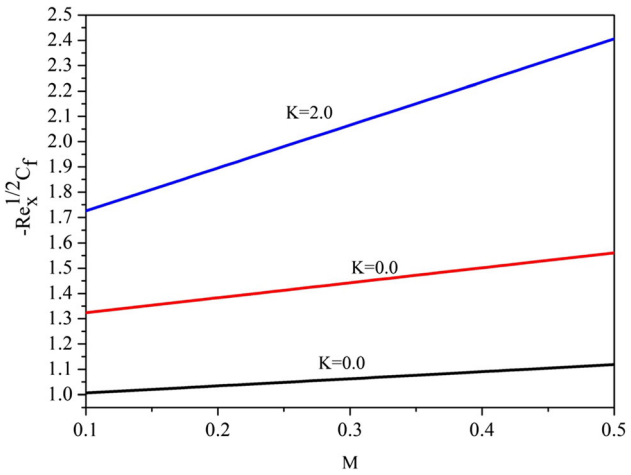

Fig. 4 Effect of K and M on friction factor

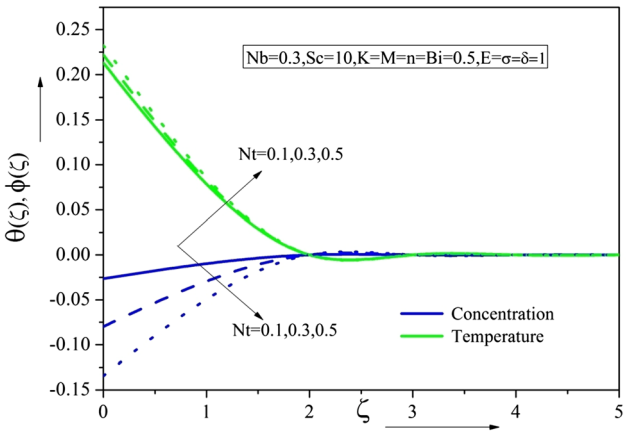

Fig. 5 Effect of Nt on temperature and concentration fields

The curves of temperature and concentration profiles with specific values of Nt are portrayed in Fig. 5. Greater values of Nt lead to higher temperature and its related thermal boundary layer thickness. The reason is Nt produce a stronger thermophoretic force which is accountable to transfer the nanoparticles in the ambient fluid. Moreover, it is observed that higher estimations of Nt lead to reduce the concentration profile. Figure 6 shows that larger value of Nb leads to increment in the concentration profile. This has exactly inverse behavior when the activation energy is absent.

Figures 7, 8, 9 and 10 are displayed to show the impact of Sc, E, δ and σ on concentration fields. It is observation from Fig. 7 that an increment of Sc leads to stronger concentration. As we know that Sc is based on Brownian diffusivity. Thus, an enhancement in Sc corresponds to decrease in Brownian diffusivity which leads to lower concentration field. Figure 8 presents the effect of E on $\phi(\zeta)$. An increment of activation energy E gives stronger concentration and its related layer thickness. Influence of δ on concentration is depicted in Fig. 9. It shows that higher values of δ lead to stronger concentration field. Opposite behavior can be seen for σ which portrayed in Fig. 10.

Influence of Biot number on temperature distribution is displayed in Fig. 11. It is noticed that higher values of Bi give an increment in temperature. Physically, temperature gradient applied on the sheet wall implies the proportion representing the temperature inside a body shifts significantly while the body heats or cools over a period. Generally if $Bi < 1$, it treated as regular temperature inside the wall and $Bi > 1$ gives the irregular temperature at the wall. Further the variations of Bi and Pr on wall temperature gradient are plotted in Fig. 12. Increase in Prandtl number and Biot number enhances temperature at the wall. Higher values of Prandtl number decrease the temperature curve which is displayed in Fig. 13.

5 Concluding remarks

Here we studied the influences of activation energy, chemical reaction, convective boundary condition and passive control of nanoparticles in flow of Maxwell

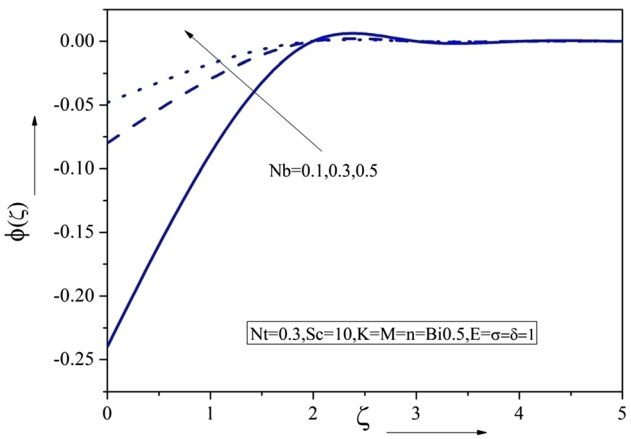

Fig. 6 Effect of Nb on concentration field

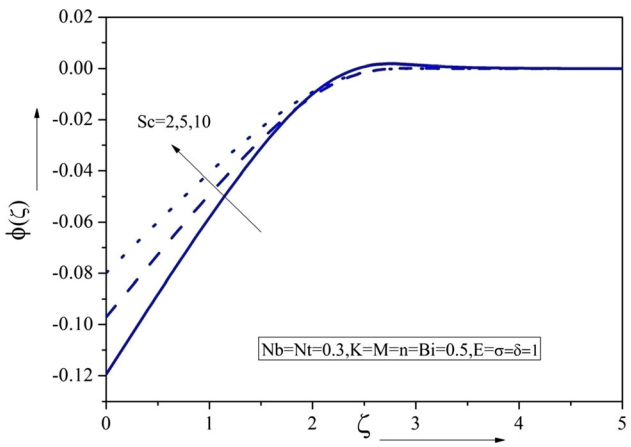

Fig. 7 Effect of Sc on concentration field

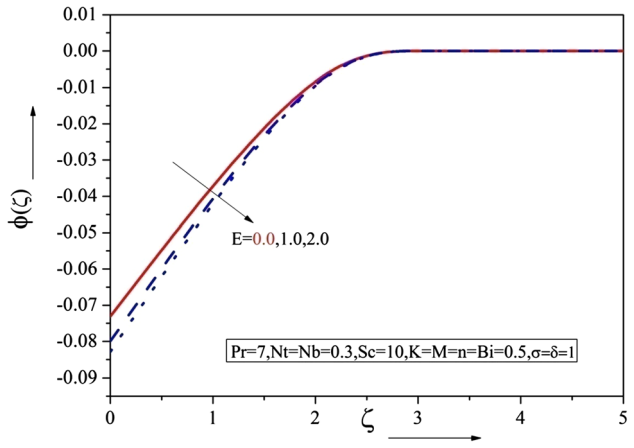

Fig. 8 Effect of E on concentration field

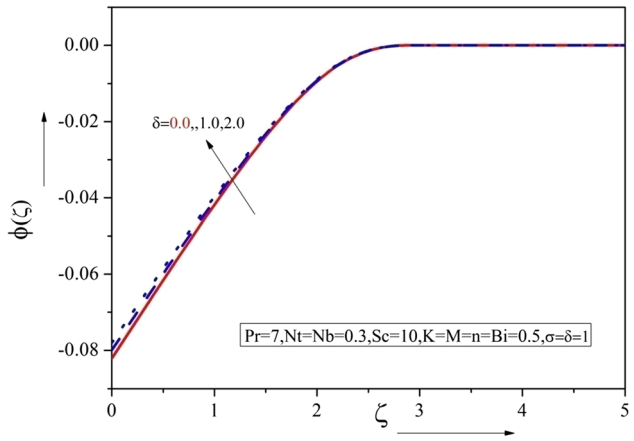

Fig. 9 Effect of δ on concentration field

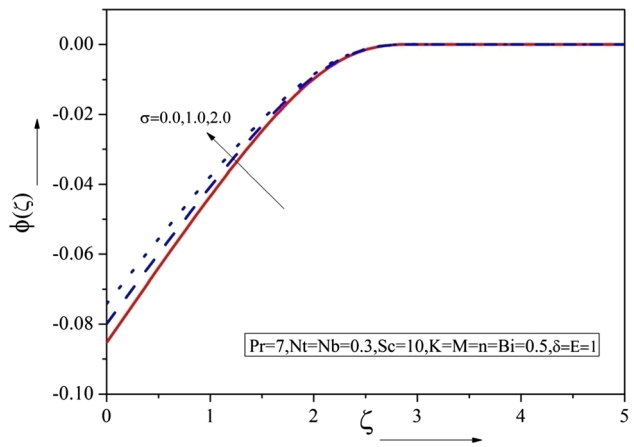

Fig. 10 Effect of σ on concentration field

magneto-nanoliquid. Activation energy can be portrayed as the tiniest required imperativeness that reactants must get before a substance reaction can happen. Mass transport process by substance reaction with approving essentialness routinely met in applications including mechanics of water

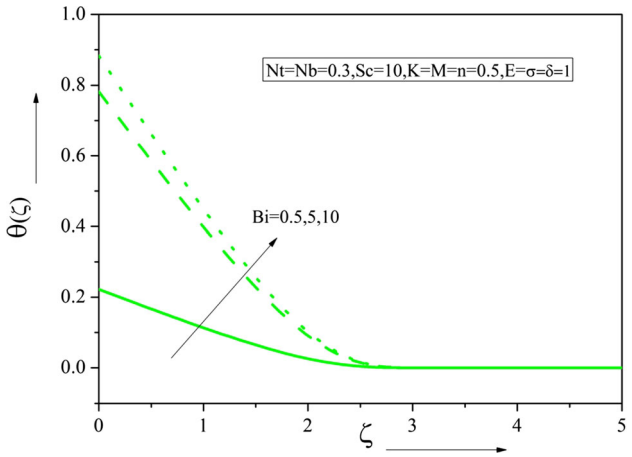

Fig. 11 Effect of Bi on concentration field

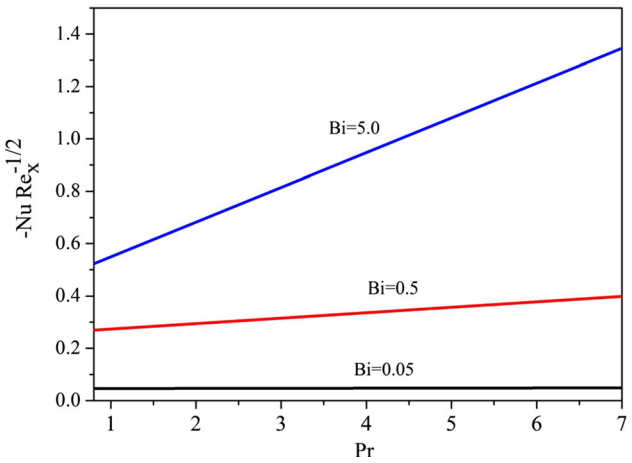

Fig. 12 Effect of Bi and Pr on wall temperature gradient

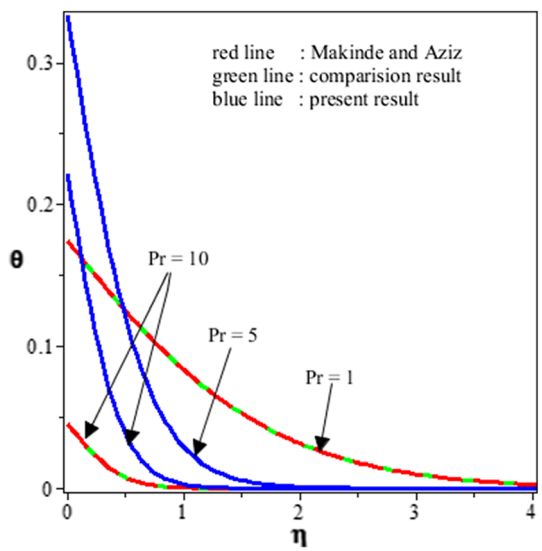

Fig. 13 Comparison of the present work with the existing work

and oil emulsions, geothermal supplies, compound portraying and sustenance getting ready. Present problem has a great application in engineering and technological field for example geothermal reservoirs, water mechanism and food processing.

Major findings are recorded as:

- Increment in elastic parameter leads to stronger velocity field but inverse effect for Hartmann number.
- Higher values of Brownian diffusion parameter promotes the concentration field but reverse effect via thermophoresis parameter.
- Increase in Schmidt number, reaction parameter and temperature difference parameter enhances the concentration field but opposite behavior for activation energy.
- Effects of Prandtl and Biot number on temperature are similar qualitatively.

Compliance with ethical standards

Conflict of Interest The authors declare that they have no conflict of interest.

References

1. Fetecau C, Fetecau C (2003) A new exact solution for the flow of a Maxwell fluid past an infinite plate. Int J Non-Linear Mech 38:423–427
2. Waheed SE (2016) Flow and heat transfer in a Maxwell liquid film over an unsteady stretching sheet in a porous medium with radiation. Springer Plus 5:1061
3. Mustafa M, Mushtaq A, Hayat T, Alsaedi A (2016) Non-aligned MHD stagnation-point flow of upper-convected Maxwell fluid with nonlinear thermal radiation. Neural Comput Appl
4. Noor NFM, Haq R, Abbasbandy S, Hashim I (2016) Heat flux performance in a porous medium embedded Maxwell fluid flow over a vertically stretched plate due to heat absorption. J Nonlinear Sci Appl 9:2986–3001
5. Mushtaq A, Abbasbandy S, Mustafa M, Hayat T, Alsaedi A (2016) Numerical solution for Sakiadis flow of upper-convected Maxwell fluid using Cattaneo–Christov heat flux model. AIP Adv 6:015208
6. Cao L, Si X, Zheng L (2016) Convection of Maxwell fluid over stretching porous surface with heat source/sink in presence of nanoparticles: lie group analysis. Appl Math Mech 37:433–442
7. Ramesh GK, Gireesha BJ (2014) Influence of heat source/sink on a Maxwell fluid over a stretching surface with convective boundary condition in the presence of nanoparticles. Ain Shams Eng J 5:991–998
8. Ramesh GK, Gireesha BJ, Hayat T, Alsaedi A (2016) Stagnation point flow of Maxwell fluid towards a permeable surface in the presence of nanoparticles. Alex Eng J 55:857–865
9. Khan MI, Khan MI, Waqas M, Hayat T, Alsaedi A (2017) Chemically reactive flow of Maxwell liquid due to variable thicked surface. Int Commun Heat Mass Transfer 86:231–238
10. Choi SUS, Eastman JA (1995) Enhancing thermal conductivity of fluids with nanoparticles. In: ASME International Mechanical Engineering Congress & Exposition, vol 66, San Francisco, pp 99–105, 12-17 November 1995
11. Buongiorno J (2006) Convective transport in nanofluids. J Heat Transfer 128:240–250
12. Ferdows M, Chapal SM, Afify AA (2014) Boundary layer flow and heat transfer of a nanofluid over a permeable unsteady stretching sheet with viscous dissipation. J Eng Thermophys 23:216–228
13. Ramesh GK (2015) Numerical study of the influence of heat source on stagnation point flow towards a stretching surface of a Jeffrey nanoliquid. J Eng 2015:10
14. Anwar MI, Shafie S, Kasim ARM, Salleh MZ (2016) Radiation effect on MHD stagnation-point flow of a nanofluid over a nonlinear stretching sheet with convective boundary condition. Heat Transfer Res 47:797–816
15. Ibrahim W (2016) Passive control of nanoparticle of micropolar fluid past a stretching sheet with nanoparticles, convective boundary condition and second-order slip. Proc Inst Mech Eng Part E J Process Mech Eng 231:704–719
16. Madhu M, Kishan N, Chamkha AJ (2017) Unsteady flow of a Maxwell nanofluid over a stretching surface in the presence of magnetohydrodynamic and thermal radiation effects. Propuls Power Res 6:31–40
17. Qayyum S, Hayat T, Alsaedi A (2017) Chemical reaction and heat generation/absorption aspects in MHD nonlinear convective flow of third grade nanofluid over a nonlinear stretching sheet with variable thickness. Results Phys 7:2752–2761
18. Javed T, Mehmood Z, Abbas Z (2017) Natural convection in square cavity filled with ferrofluid saturated porous medium in the presence of uniform magnetic field. Physica B 506:122–132
19. Sheikholeslami M, Shamlooei M (2017) Convective flow of nanofluid inside a lid driven porous cavity using CVFEM. Physica B 521:239–250
20. Waqas M, Hayat T, Shehzad SA, Alsaedi A (2018) Transport of magnetohydrodynamic nanomaterial in a stratified medium considering gyrotactic microorganisms. Physica B 529:33–40
21. Halim NA, Sivasankaran S, Noor NFM (2017) Active and passive controls of the Williamson stagnation nanofluid flow over a stretching/shrinking surface. Neural Comput Appl 28:1023–1033
22. Ramly NA, Sivasankaran S, Noor NFM (2017) Zero and nonzero normal fluxes of thermal radiative boundary layer flow of nanofluid over a radially stretched surface. Sci Iran 24:2895–2903
23. Sheikholeslami M (2017) Lattice Boltzmann method simulation for MHD non-Darcy nanofluid free convection. Physica B 516:55–71
24. Sheikholeslami M, Darzi M, Sadoughi MK (2018) Heat transfer improvement and pressure drop during condensation of refrigerant-based nanofluid; an experimental procedure. Int J Heat Mass Transf 122:643–650
25. Sheikholeslami M, Rokni HB (2018) CVFEM for effect of Lorentz forces on nanofluid flow in a porous complex shaped enclosure by means of non-equilibrium model. J Mol Liq 254:446–462
26. Bai Y, Liu X, Zhang Y, Zhang M (2016) Stagnation-point heat and mass transfer of MHD Maxwell nanofluids over a stretching surface in the presence of thermophoresis. J Mol Liq 224:1172–1180
27. Sheikholeslami M (2017) Lattice Boltzmann method simulation for MHD non-Darcy nanofluid free convection. Physica B 516:55–71
28. Khan MI, Hayat T, Khan MI, Alsaedi A (2018) Activation energy impact in nonlinear radiative stagnation point flow of Cross nanofluid. Int Commun Heat Mass Transfer 91:216–224
29. Hayat T, Qayyum S, Shehzad SA, Alsaedi A (2017) Simultaneous effects of heat generation/absorption and thermal radiation in

magnetohydrodynamics (MHD) flow of Maxwell nanofluid towards a stretched surface. Results Phys 7:562–573
30. Khan MI, Alsaedi A, Shehzad SA, Hayat T (2017) Hydromagnetic nonlinear thermally radiative nanoliquid flow with Newtonian heat and mass conditions. Results Phys 7:2255–2260
31. Makinde OD, Olanrewaju PO, Charles WM (2011) Unsteady convection with chemical reaction and radiative heat transfer past a flat porous plate moving through a binary mixture. Afrika Mathematica 22:65–78
32. Maleque KA (2013) Effects of exothermic/endothermic chemical reactions with Arrhenius activation energy on MHD free convection and mass transfer flow in presence of thermal radiation. J Thermodyn 2013:11
33. Awad FG, Motsa S, Khumalo M (2014) Heat and mass transfer in unsteady rotating fluid flow with binary chemical reaction and activation energy. PLoS ONE 9:e107622
34. Abbas Z, Sheikh M, Motsa SS (2016) Numerical solution of binary chemical reaction on stagnation point flow of Casson fluid over a stretching/shrinking sheet with thermal radiation. Energy 95:12–20
35. Shafique Z, Mustafa M, Mushtaq A (2016) Boundary layer flow of Maxwell fluid in rotating frame with binary chemical reaction and activation energy. Results Phys 6:627–633
36. Mustafa M, Khan JA, Hayat T, Alsaedi A (2017) Buoyancy effects on the MHD nanofluid flow past a vertical surface with chemical reaction and activation energy. Int J Heat Mass Transf 108:1340–1346
37. Aziz A (2009) A similarity solution for laminar thermal boundary layer over a flat plate with a convective surface boundary condition. Commun Nonlinear Sci Numer Simul 14:1064–1068
38. Ramesh GK, Gireesha BJ, Gorla RSR (2015) Boundary layer flow past a stretching sheet with fluid-particle suspension and convective boundary condition. Heat Mass Transfer 51:1061–1066
39. Nayak MK, Akbar NS, Tripathi D, Pandey VS (2017) Three dimensional MHD flow of nanofluid over an exponential porous stretching sheet with convective boundary conditions. Therm Sci Eng Prog 3:133–140
40. Hayat T, Muhammad T, Ahmad B, Shehzad SA (2016) Impact of magnetic field in three-dimensional flow of Sisko nanofluid with convective condition. J Magn Magn Mater 413:1–8
41. Hayat T, Ullah I, Ahmed B, Alsaedi A (2017) MHD mixed convection flow of third grade liquid subject to non-linear thermal radiation and convective condition. Results Phys 7:2804–2811
42. Ramesh GK, Gireesha BJ, Gorla RSR (2015) Study on Sakiadis and Blasius flows of Williamson fluid with convective boundary condition. Nonlinear Eng 4:215–221
43. Kandasamy R, Muhaimin I (2013) R. Mohamad., Thermophoresis and Brownian motion effects on MHD boundary-layer flow of a nanofluid in the presence of thermal stratification due to solar radiation. Int J Mech Sci 70:146–154
44. Makinde OD, Aziz A (2011) Boundary layer flow of a nanofluid past a stretching sheet with a convective boundary condition. Int J Therm Sci 50:1326–1332
45. Halim NA, Haq RU, Noor NFM (2017) Active and passive controls of nanoparticles in Maxwell stagnation point flow over a slipped stretched surface. Meccanica 52:1527–1539